Rigosertib induces mitotic arrest and apoptosis in RAS-mutated rhabdomyosarcoma and neuroblastoma

Joshua T. Kowalczyk[1], Xiaolin Wan[1], Edjay R. Hernandez[1], Ruibai Luo[1], Gaelyn C. Lyons[1], Kelli M. Wilson[2], Devorah C. Gallardo[1], Kristine A. Isanogle[3], Christina M. Robinson[3], Arnulfo Mendoza[1], Christine M. Heske[1], Jinqui-Qiu Chen[1], Xiaoling Luo[1], Alexander E. Kelly[1], Simone Difilippantinio[3], Robert W. Robey[1], Craig J. Thomas[2], Dan L. Sackett[4], Deborah K. Morrison[5], Paul A. Randazzo[1], Lisa M. Miller Jenkins[1], and Marielle E. Yohe[1,*]

[1] National Cancer Institute, Bethesda, MD, 20892
[2] National Center for Advancing Translational Sciences, Rockville, MD, 20850
[3] Laboratory Animal Sciences Program, Frederick National Laboratory for Cancer Research, Frederick, MD 21702
[4] Eunice Kennedy Shriver National Institute of Child Health and Human Development, Bethesda, MD, 20892
[5] National Cancer Institute, Frederick, MD, 21701

* To whom correspondence shall be addressed
Marielle Yohe
10 Center Drive
Bethesda, MD 20892
(240) 760-7346
yoheme@mail.nih.gov

Running title: Efficacy of rigosertib in rhabdomyosarcoma and neuroblastoma
Keywords: RAS, rigosertib, neuroblastoma, rhabdomyosarcoma

Conflict of Interest: This work was partially funded through a CRADA with Onconova Therapeutics Inc. (PA) to MEY.

ABSTRACT

Relapsed pediatric rhabdomyosarcomas (RMS) and neuroblastomas (NB) have a poor prognosis despite multi-modality therapy. In addition, the current standard of care for these cancers includes vinca alkaloids that have severe toxicity profiles, further underscoring the need for novel therapies for these malignancies. Here, we show that the small molecule rigosertib inhibits the growth of RMS and NB cell lines by arresting cells in mitosis, which leads to cell death. Our data indicate that rigosertib, like the vinca alkaloids, exerts its effects mainly by interfering with mitotic spindle assembly. While rigosertib has the ability to inhibit oncogenic RAS signaling, we provide evidence that rigosertib does not induce cell death through inhibition of the RAS pathway in RAS-mutated RMS and NB cells. However, the combination of rigosertib and the MEK inhibitor trametinib, which has efficacy in RAS-mutated tumors, synergistically inhibits the growth of an RMS cell line, suggesting a new avenue for combination therapy. Importantly, rigosertib treatment delays tumor growth and prolongs survival in a xenograft model of RMS. In conclusion, rigosertib, through its impact on the mitotic spindle, represents a potential therapeutic for RMS.

INTRODUCTION

Rigosertib (ON 01910.Na) is a novel, benzyl styryl sulfone compound originally developed as a non-ATP competitive, multi-kinase inhibitor. Rigosertib induces apoptosis and cell cycle arrest in many human cancer cell lines, including those derived from breast cancer, prostate cancer, glioblastoma multiforme, non-small cell lung cancer, gastric cancer, colorectal cancer, melanoma, head and neck squamous cell carcinoma, myelodysplastic syndrome, mantle cell lymphoma, pancreatic cancer, chronic lymphocytic leukemia and chronic myelogenous leukemia patients. Importantly, rigosertib has a minimal effect on normal human cells, including HUVEC (1).

The precise mechanism of action of rigosertib has remained elusive despite rigorous investigation. Early reports described rigosertib as a direct inhibitor of Polo-like kinase-1 (PLK1), although this effect has not been validated through subsequent studies (1). Recently, rigosertib has been characterized as a RAS mimetic compound, capable of binding to the RAS-binding domains of RAS effectors, such as the Raf family members (ARAF, BRAF and RAF1) and PI3 kinase isoforms (p110 α and β), thus blocking the interaction with active RAS (2). In this way, rigosertib decreases signaling through the RAS/RAF/MEK/ERK mitogen-activated protein (MAP) kinase and the PI3 kinase/AKT/mTOR pathways. Rigosertib also induces mitotic and oxidative stress, which activates the stress MAP kinases, p38 and JNK. The stress MAP kinases phosphorylate components of the RAS pathway, including Raf family members and SOS1, a RAS guanine nucleotide exchange factor, which further decreases signaling through the RAS/RAF/MEK/ERK MAP kinase pathway (3). The mitotic stress induced by rigosertib may be due to the fact that rigosertib, or a degradation product of rigosertib, binds to an intradimer site between α- and β-tubulin in a manner similar to colchicine, which prevents microtubule growth (4-6).

Functionally, rigosertib has been shown to have anticancer effects across a range of malignancies both preclinically and clinically. Rigosertib is a potent inhibitor of tumor growth in HCT116 and A549 xenograft models of RAS-mutated colorectal and lung adenocarcinoma, respectively, and represses the growth of RAS-mutated pancreatic intraepithelial neoplasia in a genetically engineered mouse model (2). Rigosertib also suppresses extramedullary hematopoiesis in a *KRAS*^{G12D}-driven model of the pediatric myeloproliferative neoplasm, juvenile myelomonocytic leukemia (JMML) (7). Clinically, rigosertib has shown efficacy in trials for adults with a variety of solid tumors, with complete or partial responses noted in subjects

with thymic carcinoma, pancreatic ductal adenocarcinoma and head and neck squamous cell carcinoma (8-10). Rigosertib also has been efficacious in hematologic malignancies, particularly Hodgkin lymphoma and high-risk myelodysplastic syndrome (11-13). No studies evaluating the efficacy of rigosertib in patients with RAS-mutated cancers have been conducted to date. However, in patients with metastatic pancreatic adenocarcinoma, tumors primarily driven by mutations in KRAS, the combination of rigosertib and gemcitabine failed to show an improvement in survival or response compared to gemcitabine alone (14).

RAS is a common driver of pediatric cancers, including solid tumors, such as PAX-fusion negative rhabdomyosarcoma (FN-RMS) (15), malignant peripheral nerve sheath tumor (16), relapsed neuroblastoma (NB) (17), and malignant ectomesenchymoma (18), as well as hematologic malignancies such as JMML (19). In the current study, we aimed to investigate the activity of rigosertib in models of FN-RMS and NB that harbor mutations in one of the RAS isoforms, *HRAS*, *KRAS*, or *NRAS*. FN-RMS and NB are both embryonal tumors, with cells of origin being skeletal muscle (20) and sympathoadrenal precursors (21), respectively. We also aimed to identify the mechanism of action of rigosertib in the context of pediatric solid tumors in order to identify appropriate biomarkers for pharmacodynamic studies in future clinical trials of rigosertib for pediatric patients.

MATERIALS AND METHODS

Cell lines and reagents: The RMS cell lines RD, SMS-CTR, BIRCH, RH4, RH30, RH18 and RMS-YM were obtained from J. Khan. The NB cell lines SKNAS, NBEB, SHEP, SY5Y, and IMR5 were obtained from C. Thiele. CHP212 was obtained from the Childhood Cancer Repository. The RASless MEFs were obtained through collaboration with the NCI RAS initiative. All cell lines were confirmed to be mycoplasma negative using the MycoAlert kit (Lonza) and their identity was confirmed by STR fingerprinting prior to experimental use. BIRCH, RMS-YM, RH18, SKNAS, NBEB, SHEP, SY5Y, and IMR5 were grown in RPMI with 10% FBS. The other cell lines were grown in DMEM with 10% FBS. Trametinib was obtained from the NIH Developmental Therapeutics Program (DTP, RRID:SCR_003057). Rigosertib was obtained through a Cooperative Research and Development Agreement (CRADA) with Onconova Therapeutics (PA). Biotinylated rigosertib and ON0911 were a gift of P. Reddy. DAPI (D1306) was obtained from Thermo. N-acetylcysteine (A9165), biotin (B4501), and menadione (M2518) were obtained from Sigma. SB-203580 (S1076) (22), nocodazole (S2775),

albendazole (S1640), and combretastatin A4 (S7783) (23) were obtained from SelleckChem. Vincristine was obtained from the NIH Division of Veterinary Resources (DVR) veterinary pharmacy.

Immunofluorescence: Cells plated on fibronectin coated coverslips (10 μg/ml) were treated as indicated and fixed with 4% paraformaldehyde in phosphate buffered saline (PBS). Cells were permeabilized with PBS containing 0.5% Triton X-100 for 10 minutes and then washed three times with PBS containing 0.1% Triton X-100. The cells were then incubated in PBS with 0.1% Triton X-100, 2% bovine serum albumin and 0.1% sodium azide (blocking buffer) for 10 min at 4°C. Cells were incubated at room temperature for 1 hour with primary antibodies (Supplemental Table 1) diluted in blocking buffer. Cells were washed four times with blocking buffer and then incubated for 1 hr at room temperature with secondary antibody (Supplemental Table 1) diluted 1:200 in blocking buffer. Cells were washed four times with PBS containing 0.1% Triton X-100 and once with PBS. The cells were then incubated with 300 nM DAPI for 5 to 10 min and rinsed three times with PBS. The coverslips were mounted with Dako Fluorescence mounting medium. Microscope images were captured using a Leica SP8 laser-scanning confocal microscope using a 63X, 1.4 numerical aperture objective (Leica Microsystems Inc, Buffalo Grove, IL). Stacks of 0.3 μm slices were collected. Maximum projection images are presented. Image analysis was performed in ImageJ (RRID:SCR_003070).

Rigosertib pull down and mass spectrometry: RD cells in the logarithmic growth phase were lysed in PBS with added 0.15% Tween 20, 1 mM DTT and HALT protease/phosphatase inhibitors. Nuclei were lysed by passing the cell lysate through a 20G syringe five times. The resulting whole cell lysates were clarified by centrifugation at 16,000 rpm at 4°C for 10 minutes. Approximately 1 μg of total lysate was used per condition. 50 μM of free biotin, biotinylated rigosertib, or biotinylated ON01911 was added to the cell lysate. The samples were incubated at 4°C for 2 hours prior to the addition of 50 μL NeutrAvidin beads (Thermo). The bead: lysate slurries were incubated on an end-over-end rotator overnight at 4°C. Beads were washed three times in PBS prior to resuspension in LDS sample buffer (Thermo). Denatured samples were separated by SDS-PAGE for in-gel trypsin digestion as described (24). For mass spectrometry analysis, peptides were trapped on a trapping column and separated on a 75 μm x 15 cm, 2 μm Acclaim PepMap reverse phase column (Thermo) using an UltiMate 3000 RSLCnano HPLC (Thermo). Peptides were separated at a flow rate of 300 nL/min followed by online analysis by

tandem mass spectrometry using a Thermo Orbitrap Fusion mass spectrometer. Parent full-scan mass spectra were collected in the Orbitrap mass analyzer set to acquire data at 120,000 FWHM resolution; ions were then isolated in the quadrupole mass filter, fragmented within the HCD cell (HCD normalized energy 32%, stepped ± 3%), and the product ions analyzed in the ion trap. Proteome Discoverer 2.2 (Thermo, RRID:SCR_014477) was used to search the data against human proteins from the UniProt database (RRID:SCR_004426) using SequestHT. The search was limited to tryptic peptides, with maximally two missed cleavages allowed. Cysteine carbamidomethylation was set as a fixed modification, and methionine oxidation set as a variable modification. The precursor mass tolerance was 10 ppm, and the fragment mass tolerance was 0.6 Da. The Percolator node (RRID:SCR_00287) was used to score and rank peptide matches using a 1% false discovery rate.

Cell growth assay: Dose-response, matrix, and time-course viability curves were generated by quantifying percent cell confluence from phase contrast images of cells in 384-well plates. Images were taken every 4 hours using an Incucyte ZOOM (Essen Bioscience). Cells were plated to achieve 20% confluence at the time of drug dosing. Each condition was assayed in triplicate. IC50 values were calculated using GraphPad Prism version 7 (RRID:SCR_002798). Synergy was calculated according to the Bliss Independence model (25).

Clonogenic assay: RD, SMS-CTR, RH30, SKNAS, or CHP212 cells were plated at a density of 100 cells per well in 6-well tissue culture plates. The plates were incubated for 2 weeks before fixing in 10% formaldehyde and staining with 0.01% crystal violet.

Annexin V assay: RD or SMS-CTR cells were treated with vehicle (DMSO) or 2 μM rigosertib for 48 hours prior to harvesting and incubating with APC-labeled human recombinant annexin V (BioLegend) and Sytox Green (Thermo) according to the manufacturers' instructions. Samples were read on a FACSCanto flow cytometer (BD Biosciences) and percent annexin positive cells were calculated in FlowJo (RRID:SCR_008520).

Xenograft experiments: Xenograft studies were approved by the Animal Care and Use Committee (ACUC) of the NCI-Bethesda or the Frederick National Laboratory for Cancer Research (FNLCR). FNLCR is accredited by AAALAC International and follows the Public Health Service Policy for the Care and Use of Laboratory Animals. Animal care was provided in accordance with the procedures outlined in the *Guide for the Care and Use of Laboratory Animals*. SCID beige mice were purchased from Charles River laboratories. All animals were female, and all were injected at 4-8 weeks of age. For the RD rigosertib experiment, 2 million cells were injected orthotopically into the gastrocnemius muscle in the left hind leg of 13 SCID-

Beige mice. After 3 weeks, the mice were randomized into vehicle (n=6) and rigosertib (n=7) groups (equivalent tumor size in each group). Rigosertib was prepared daily in PBS and stored at 4°C until use. The treatment group mice received rigosertib at a dose of 150 mg/kg (100 µL of a 30 mg/mL solution) by intraperitoneal injection twice daily 5 days per week; the vehicle group received the same volume of vehicle by intraperitoneal injection twice daily 5 days per week. Mice received rigosertib until they reached study endpoint. For the RD vincristine experiment, 2 million cells were injected as above. The mice were randomized into vehicle and vincristine groups with 10 mice per group. The vincristine group received 1 mg/kg weekly via tail vein injection. Vincristine was diluted in PBS immediately prior to injection. Mice received vincristine or vehicle for a period of 28 days at which time the treatment was stopped, and the mice were observed for tumor development. For the SKNAS experiment, 2 million cells were injected subcutaneously in the left flank of 9 SCID beige mice. After 2 weeks, the mice were randomized into vehicle (n=4) and rigosertib (n=5) groups and treated as described for mice bearing RD tumors.

In all experiments, the tumor dimensions were measured twice a week with digital calipers to obtain two diameters of the tumor sphere, from which the tumor volume was determined using the equation $(D \times d^2)/6 \times 3.14$ (where D = the maximum diameter and d = the minimum diameter) (26). For the IM injections, the whole hindlimb was measured while for the SQ injections the tumor itself was measured. Animals were euthanized when they reached tumor endpoint, which was defined as when the tumor measured greater than 18 mm in any direction for the IM injected tumors and 20 mm in any direction for the SQ injected tumors. Animals were also euthanized if the tumors showed signs of ulceration or caused significant discomfort to the animal, in accordance with the humane endpoints recommended by our institutional ACUC.

Capillary Immunoassays: Cell lysates were prepared in MPER (Thermo). Fresh frozen tumor samples were prepared in TPER (Thermo) using a TissueRuptor. Cell or tumor lysates were mixed with 1x sodium dodecyl sulfate master mix containing sample buffer (ProteinSimple) dithiothreitol, and fluorescently labeled standards (ProteinSimple) and were heated at 70˚C for 10 minutes before being loaded into Peggy Sue instrument (ProteinSimple) for analysis. During electrophoresis, proteins were separated by molecular weight while migrating through the separation matrix (ProteinSimple). Separated proteins were immobilized on the capillary wall using UV light, and incubated with a blocking reagent (ProteinSimple), followed by immunoprobing with respective primary antibodies and HRP conjugated anti-rabbit or anti-mouse secondary antibodies (ProteinSimple, Jackson ImmunoResearch). A 1:1 mixture of

luminol and peroxide (ProteinSimple) was added to generate chemiluminescence, which was captured by a CCD camera. The digital image was analyzed by Compass software (ProteinSimple, RRID:SCR_015874). Target protein quantities were determined by quantifying the signal strength (peak area). The Simple Western total protein assay was employed as a loading control. In the total protein analysis module, proteins were separated by MW and immobilized in the capillary, prior to incubation with biotinylating reagent (ProteinSimple), followed by HRP-streptavidin (ProteinSimple) for chemiluminescent detection.

DNA content analysis: Cells were fixed with 70% ethanol prior to staining with propidium iodide/TritonX-100 (Thermo). Stained cells were analyzed using a Sony SA3800 instrument at the CCR Flow Cytometry Core facility. Cell cycle analysis was performed in ModFit LT version 5 using default parameters.

Immunoblot experiments: Antibodies used in this study are listed in Supplemental Table 1. Cells in culture were washed twice with ice cold PBS prior to lysis in lysis buffer (Cell Signaling Technologies) with added HALT protease and phosphatase inhibitors (Thermo). Cells were lysed at 4°C for 10 minutes and the resulting lysates were clarified by centrifugation at 16,000 rpm at 4°C for 10 minutes. Protein concentration of the resulting supernatant was estimated by BCA assay (Thermo). 10-40 µg of sample were run on NuPage 4-12% BisTris minigels (Novex) and transferred to PVDF membranes (Amersham). Membranes were blocked in 5% nonfat dried milk in TBST for 1 hour at room temperature and incubated with primary antibodies overnight at 4°C. HRP-conjugated anti-rabbit or mouse antibodies (Cell Signaling Technologies) were used as secondary antibodies, as indicated in Supplemental Table 1. Protein was visualized using SuperSignal West Femto maximum sensitivity substrate (Thermo) on a ChemiDoc imager (BioRad).

Caspase-Glo 3/7 Assay: Cells were plated at a density of 10 - 20,000 cells/well in 96-well plates. The next day, cells were treated with DMSO, 2 μM rigosertib, 10 mM NAC, and 20 mM SB-203580 both individually and in combination for 24 hours. The caspase-Glo 3/7 assay (Promega) protocol was followed per manufacturer's recommendations. Luminescence was read on a SpectraMax M5 (Molecular Devices).

ROS-Glo Assay: RD or SMS-CTR cells were plated at a density of 10,000 cells/well in 96-well plates. Media alone (no cells) was also plated as a negative control. The next day, cells or media were treated with DMSO, 2 μM rigosertib, or 50 μM menadione for 24 hours. The ROS-

glo protocol (Promega) was followed per the manufacturer's instructions. Luminescence was read on a SpectraMax M5 (Molecular Devices).

Intracellular Tubulin Polymerization Assay: RD and SKNAS cells were plated at a density of 500,000 cells per well in 6-well dish 24 hours prior to treatment with increasing concentrations of rigosertib. After 4 hours of rigosertib treatment, the cells were lysed in a hypotonic lysis buffer (1 mM MgCl2, 2 mM EGTA, 20 mM Tris HCl pH 6.8, 0.15% IGEPAL, 5 mM taxol) for 10 min at 37°C as previously described (27). The cell lysates were centrifuged at 15,000 rpm for 10 minutes at room temperature. The resulting supernatants (S), containing soluble tubulin, were removed and the resulting pellets (P), containing polymerized tubulin, were resuspended in a volume of hypotonic lysis buffer equivalent to the removed supernatant. Equal volumes of S and P for each treatment condition were subjected to SDS-PAGE followed by immunoblotting for α-tubulin. Band densities were quantified using ImageJ.

High Throughput Cell Viability Assays: A total of 130 cancer cell lines were previously screened against rigosertib, which is a component of various NCATS compound libraries (28,29). The majority (87) of these cell lines express wild-type RAS, while a subset (42) express either an HRAS, KRAS, or NRAS mutant. Potency was determined in 1536-well tissue culture plates preplated with 11 concentrations of rigosertib. Cells were grown in the presence of rigosertib for 48 hours prior to the addition of CellTiter Glo (Promega) to assess cell viability. Luminescent signal was measured on a ViewLux instrument and data was normalized to DMSO treated wells as 100% viability and no cells controls as 0% viability. The area under the curve (AUC) from the resultant 11-point dose response curves was calculated using a standard trapezoidal method. The AUCs were z-transformed to compare the activity of rigosertib to that of the other compounds within that library for each cell line, such that a negative z-score denotes greater potency. This integration and harmonization of screening data was carried out in Palantir Foundry, through the NIH Integrated Data Analysis Platform (NIDAP).

RESULTS

Rigosertib potently decreases the proliferation of RMS and NB cell lines

To determine the efficacy of rigosertib in RMS and NB cell lines, we investigated the effects of increasing concentrations of rigosertib on cell confluence using live cell imaging. Cell lines with

and without RAS mutations were used in this analysis (Supplemental Table 2). Importantly, in the cell lines used, the presence of a mutation in a RAS isoform confers a functional dependency on that RAS isoform (30). The IC50 of rigosertib in RMS (Figure 1A) and NB (Figure 1B) cell lines was determined to be in the submicromolar range using this assay. However, no statistically significant difference in IC50 was observed between cell lines harboring a mutation in a RAS isoform (HRAS, KRAS, or NRAS) and those expressing wild type RAS. To confirm that rigosertib efficacy is independent of RAS mutation status, we also investigated the efficacy of rigosertib in a panel of isogeneic RAS-dependent MEFs obtained from the NCI RAS Initiative (Figure 1C). These MEFs were derived from NRAS- and HRAS-null mice, and the endogenous KRAS allele was subsequently removed via Cre-Lox-mediated recombination. These RASless MEFs were then transduced with wild type KRAS4b, $KRAS4b^{G12V}$ or $BRAF^{V600E}$, with the resulting MEF lines being dependent upon their respective transgene for proliferation (31). Rigosertib was equally potent at inhibiting cell viability in MEFs expressing either wild-type KRAS4b, $KRAS4b^{G12V}$, or importantly $BRAF^{V600E}$, which lacks expression of any of the RAS isoforms, validating that the activity of rigosertib does not depend on RAS status. In addition to the efficacy observed in a short-term assay of cell viability, rigosertib treatment also inhibited cell growth in a 14-day clonogenic assay in RAS-mutated RMS (RD, SMS-CTR), RMS cells expressing wild-type RAS (RH30) and RAS-mutated NB (CHP212, SKNAS) cell lines (Figure 1D). In the clonogenic experiments, the NB cells appeared to be more sensitive to rigosertib than the RMS cells. To extend our analysis, we compared the potency of rigosertib in additional pan-cancer RAS wild-type and RAS mutant cell lines that have been subjected to a high-throughput drug screen at the National Center for Advancing Translational Sciences. Potency in this screen is represented as the cell viability area under the dose response curve (AUC). In this dataset, there was no difference in potency for rigosertib in RAS wild-type or RAS-mutant cell lines; however, the MEK inhibitor, trametinib, was more potent (had a lower AUC) in RAS-mutant as compared to RAS wild-type cells (Figure 1E). Taken together, the above results suggest that the effects of rigosertib on cell viability are independent of mutant RAS expression.

Rigosertib induces apoptosis and mitotic arrest in RMS and NB cell lines

To determine the mechanism by which rigosertib affects RMS and NB cell line viability, we tested whether rigosertib was able to induce apoptosis in these cells. Rigosertib induced caspase 3/7 activity (Figure 2A) and phosphatidylserine externalization as detected by annexin V staining (Figure 2B) in RAS-mutant RMS cell lines, RD and SMS-CTR, suggesting apoptosis

was induced in these cells. Caspase 3/7 activity was also induced by rigosertib in RAS wild-type FN-RMS cell lines, RMS-YM and RH18 (Supplemental Figure 1A), as well as RAS mutant (SKNAS and NBEB) and RAS wild-type (SHEP and SY5Y) NB cell lines (Supplemental Figure 1B). However, rigosertib also induced G2/M arrest in RMS and NB cells, as determined by DNA content analysis (Figure 2C), suggesting that the rigosertib effects in these cell lines are both cytotoxic and cytostatic. To further characterize the cell cycle block induced by rigosertib, we determined the effect of rigosertib on histone H3 S10 phosphorylation, which is a marker specific for cells in mitosis. Rigosertib increased phospho-histone H3 in both RMS and NB cells as determined by immunoblot (Figure 2D) and immunofluorescence (Figure 2E) experiments, suggesting that rigosertib arrests pediatric solid tumor cells in mitosis. The cellular effects of rigosertib were observed in SMS-CTR cells in as few as 4 hours (Supplemental Figure 1C) and were irreversible after removal of drug from the cell culture media (Supplemental Figure 1D).

Rigosertib does not inhibit signaling through RAS effectors in RMS and NB cells

To determine whether rigosertib inhibits signaling through the RAS effector pathways RAF/MEK/ERK and PI3 kinase/AKT/mTOR, we serum starved RD and SMS-CTR RMS cells, treated with vehicle (DMSO) or rigosertib, and then stimulated with either vehicle (PBS) or IGF1 (Figure 3A). IGF1 stimulation did not increase ERK phosphorylation within each treatment group because each of these cell lines harbors a RAS isoform mutation, which confers constitutive signaling through the RAF/MEK/ERK pathway. IGF1 stimulation however did increase AKT phosphorylation in serum-starved RD and SMS-CTR, suggesting that the serum starvation conditions were sufficient. Rigosertib treatment increased ERK phosphorylation but did not impact AKT phosphorylation compared to DMSO-treated cells in the serum-starved and IGF1-stimulated conditions in both cell lines. In contrast to previous studies in MDA-MB-231 cells in which rigosertib treatment induced the phosphorylation of sites that suppress MEK1 activity (T286, T292) but not those that result in MEK activation (S217,S221) (32), we found that rigosertib treatment in RD cells increased both positive and negative phosphorylation on MEK1 (Figure 3B). Co-treatment with the allosteric MEK inhibitor, trametinib, decreased MEK1 phosphorylation at T286 relative to rigosertib treatment alone. Trametinib did not impact rigosertib-induced T292 phosphorylation. Importantly, however, trametinib prevented rigosertib-induced ERK phosphorylation. Results in SKNAS were similar to those obtained in RMS lines in that IGF1 stimulation in SKNAS did not increase ERK phosphorylation but did increase AKT phosphorylation. In contrast to the results in RMS cells, rigosertib treatment did not impact ERK phosphorylation compared to DMSO-treated cells in the serum-starved or IGF1-stimulated

conditions in SKNAS (Figure 3C). Rigosertib induced positive and negative phosphorylation events on MEK1 in SKNAS, similar to the effects in the RD cell line (Figure 3D). These results suggest that rigosertib does not decrease signaling through RAS effector pathways in RMS or NB cell lines.

Because trametinib decreases ERK phosphorylation induced by rigosertib, we hypothesized that trametinib and rigosertib might synergistically inhibit RMS cell viability. To test this hypothesis, we performed a matrix viability experiment in RD cells (Figure 3E). Using the Bliss independence model, we were able to identify several conditions in which rigosertib and trametinib were synergistic. For example, the addition of 30 nM trametinib to 1 μM rigosertib prevents RD cell growth (Figure 3F). These results support the conclusion that inhibitors of the RAF/MEK/ERK pathway can synergize with rigosertib in RMS.

Rigosertib activates stress MAP kinase pathways in RMS and NB cells

Rigosertib treatment of CLL cells (33) and HeLa cells (3) activates the JNK stress MAP kinase pathway following release of mitochondrial reactive oxygen species (ROS). In HeLa cells, activated JNK phosphorylates and negatively regulates components of the RAS/RAF/MEK/ERK MAP kinase pathway. To test the hypothesis that rigosertib treatment stimulates ROS production in RMS cells, we performed a ROS-glo assay (Supplemental Figure 2A). In this experiment, rigosertib stimulated ROS production in RD to the same extent as menadione, a known stimulator of ROS production (34). The ability of rigosertib to stimulate ROS was inhibited by co-treatment with the ROS scavenger, N-acetylcysteine (NAC). Compared to RD cells, SMS-CTR cells produced less ROS as a result of either rigosertib or menadione treatment. The ability of NB cells to produce ROS as a result of rigosertib treatment was unable to be determined because of the high degree of spontaneous oxidation of the RPMI media components in which these cells are cultured.

Importantly, rigosertib treatment of RMS cells induced phosphorylation, and thus activation, of both the p38 stress MAP kinase and MKK4, the activator of the stress MAP kinase, JNK (Figure 4A). Rigosertib-induced phosphorylation of p38 and MKK4 was inhibited by co-treatment with NAC. To determine if the cytotoxic and cytostatic effects of rigosertib in RMS cells were dependent upon activation of p38, we used the pharmacologic inhibitor of p38, SB-203580. SB-203580 inhibits the kinase activity of p38, but its effect on p38 phosphorylation is cell-type dependent (35,36). Co-treatment with SB-203580 inhibited rigosertib-induced p38

phosphorylation in SMS-CTR but not RD cells. The co-treatment did inhibit rigosertib-induced phosphorylation of MAPKAPK2, a p38 substrate, in RD cells, indicating inhibition of p38 catalytic activity (Figure 4B). These data suggest that SB-203580 inhibits p38 activity in RD and SMS-CTR cells. Consistent with previous studies (3), neither NAC (Figure 4C) nor SB-203580 (Figure 4D) treatment had a significant effect on rigosertib-induced G2/M arrest, suggesting that ROS release occurs independent of the arrest in the cell cycle. In addition, neither NAC nor SB-203580 treatment prevented rigosertib-induced caspase 3/7 activity (Figure 4E and 4F) or PARP cleavage (Figure 4A and 4B).

Unlike the results in RMS cells, rigosertib did not induce phosphorylation of p38 in SKNAS or NBEB, and rigosertib induced MKK4 phosphorylation in NBEB but not SKNAS (Supplemental Figure 2B). NAC treatment had very little effect on p38, MAPKAPK2, and MKK4 phosphorylation in the presence and absence of rigosertib in both SKNAS and NBEB cells; however, SB-203580 treatment did decrease MAPKAPK2 phosphorylation in SKNAS and p38 phosphorylation in NBEB, indicating inhibition of p38 catalytic activity (Supplemental Figure 2B). NAC neither inhibited G2/M arrest due to rigosertib in SKNAS, nor inhibited rigosertib-induced caspase 3 activation in SKNAS or NBEB (Supplemental Figures 2C and 2D). SB-203580 similarly neither impacted rigosertib-induced G2/M arrest nor caspase 3 activation (Supplemental Figures 2C and 2E), consistent with the results in RMS cells. Taken together, these results suggest that rigosertib induces apoptosis in RMS and NB cells via a mechanism that is independent of the rigosertib-induced activation of the stress MAP kinase pathways.

Rigosertib interacts with tubulin in RMS and NB cells to induce mitotic spindle defects

To identify the mechanism by which rigosertib induces mitotic arrest in RMS cells, we affinity purified rigosertib-binding proteins from RD cell lysates using a biotin-rigosertib conjugate and identified the interacting proteins using mass spectrometry. Free biotin as well as a biotin conjugate of an inactive isomer of rigosertib, ON 01911, were used as negative controls in this experiment, as previously described (2). Mass spectrometry identified TUBB2A/B (β-tubulin) as a specific interactor with rigosertib but not free biotin or biotinylated ON 01911 (Supplemental Table 3). To determine whether the interaction between rigosertib and tubulin has functional relevance, we assessed levels of acetylated tubulin, a marker of microtubule stability, in RD and SKNAS cells. Acetylated tubulin was decreased in RD and SKNAS cells treated with rigosertib, as determined by quantitative capillary immunoassay (Figure 5A), indicating decreased microtubule stability in cells treated with rigosertib. Acetylated tubulin, then, represents an

appropriate pharmacodynamic marker for on-target rigosertib activity in RMS and NB. In a complimentary experiment, treatment of RD or SKNAS cells with increasing concentrations of rigosertib resulted in a dose dependent shift of tubulin from the polymerized form in the pellet fraction (P) to the soluble form (S), consistent with a destabilization of microtubules (Figure 5B). Importantly, immunofluorescence experiments in RD and SKNAS cells revealed that rigosertib treatment induces mitotic spindle defects, including a reduction of spindle length and an increase in tripolar and tetrapolar spindles (Figure 5C). These results confirm that rigosertib cytotoxicity in pediatric cancer cell lines is due, at least in part, to induction of mitotic spindle defects. Previous studies showed that rigosertib binds to the colchicine binding site at the $\alpha\beta$ tubulin intradimer interface (5). We therefore hypothesized that other tubulin-binding drugs might have efficacy in pediatric cancer cells. We screened a panel of drugs including nocodazole, albendazole, and combretastatin A4, which also bind to tubulin dimers in the colchicine binding site, for their ability to decrease proliferation in the RMS cell line, SMS-CTR (Supplemental Figure 3A). Like rigosertib, combretastatin A4 showed no selectivity for RAS mutated cells in the NCATS screening dataset (Supplemental Figure 3B). Low concentrations of combretastatin A4 also induced mitotic spindle defects in RD and SKNAS cells (Supplemental Figure 3C), indicating a similar mechanism of action to rigosertib.

Rigosertib has limited efficacy in mouse models of RMS and NB

The vinca alkaloids, which are inhibitors of tubulin polymerization, are commonly used chemotherapeutics in the treatment of pediatric RMS and NB. We hypothesized that rigosertib, functioning as an inhibitor of tubulin polymerization, might also be effective in the treatment of these pediatric cancers. To test this hypothesis, we evaluated the effect of rigosertib on *in vivo* tumor growth. In orthotopic RD xenograft models, rigosertib treatment delayed tumor growth (Supplemental Figure 4A) such that resulting tumors were smaller compared to tumors from mice treated with vehicle when measured at the end of the study (Figure 6A). This delay in tumor growth resulted in a modest survival advantage for the rigosertib-treated mice (Figure 6B). In contrast, in a separate experiment, treatment with the vinca alkaloid vincristine which has an IC_{50} of approximately 10 nM in RD cells *in vitro (37)*, prevented tumor growth in an orthotopic RD xenograft model (Supplemental Figure 4B). In addition, rigosertib did not delay tumor growth in a heterotopic SKNAS xenograft model (Supplemental Figure 4C). Importantly, no toxicity was observed in mice receiving rigosertib, including no significant body weight loss over the treatment period (Figure 6C). Pharmacodynamic assessment of tumors harvested at the study endpoint revealed that acetylated tubulin did not decrease in the tumors from mice

treated with rigosertib as compared to vehicle control tumors (Figure 6D). These results suggest that the limited efficacy of rigosertib in this model is due to early acquisition of resistance to rigosertib or poor target engagement. The cell line xenografts used in this study were grossly encapsulated and poorly vascularized, both of which could contribute to poor drug penetration.

DISCUSSION

In this study, we show that rigosertib treatment decreases viability in rhabdomyosarcoma and neuroblastoma cells. This decrease in cell viability occurs through the binding of rigosertib to tubulin, an interaction that destabilizes microtubules, and results in the induction of apoptosis and/or mitotic arrest. Mitotic arrest then stimulates production of ROS, as it does in other cellular contexts (38). ROS production stimulates the stress MAP kinase pathways; however, these pathways do not contribute to further apoptosis or inhibition of the RAS/RAF/MEK/ERK MAP kinase pathway in the RAS-mutated, RMS and NB cells used in this study. The lack of apoptosis induced by ROS production in RMS cells is not unexpected, because although skeletal muscle cells have high anti-oxidant capacity (39), extreme levels of ROS induce necrosis, not apoptosis, in skeletal muscle myoblasts, which have a similar gene expression pattern to FN-RMS cells (29). RMS is sensitive to other therapeutics that induce ROS *in vitro* and *in vivo*; however, the precise mechanism by which these agents inhibit RMS growth is not completely described (40,41). Increased levels of ROS stimulate ERK phosphorylation in myoblasts, which could explain why rigosertib stimulates rather than represses RAF/MEK/ERK MAP kinase signaling in RMS cells (42), raising the possibility that rigosertib effects could be cell type specific.

Several lines of evidence support the fact that the mechanism of action of rigosertib in pediatric cancers is not primarily RAS-dependent. First, rigosertib demonstrates no increased cytotoxicity in pediatric cancer cell lines harboring mutant RAS alleles as compared to those expressing wild-type RAS, and in fact, rigosertib was cytotoxic to MEFs devoid of RAS expression. Second, while inhibitors of components of the RAS/RAF/MEK/ERK MAP kinase pathway induce cell cycle arrest in the G1 phase in FN-RMS (29) and NB cell lines (43), rigosertib induces a mitotic phase arrest. Third, rigosertib treatment does not decrease ERK phosphorylation in these pediatric cancer cell lines.

We do not observe an interaction between biotinylated rigosertib and RAS effectors by mass spectrometry; however, this does not rule out that such an interaction is occurring. In contrast, we did observe an interaction between biotinylated rigosertib and β-tubulin in RMS cells. Several additional experiments support the hypothesis that rigosertib is functioning as a microtubule destabilizing agent in RMS and NB cells. First, rigosertib, like other microtubule destabilizing agents, induces mitotic arrest in these cells. In addition, rigosertib treatment induces mitotic spindle defects, decreases tubulin acetylation, and decreases intracellular polymerized tubulin. Therefore, although rigosertib may have a role as a RAS-mimetic in rhabdomyosarcoma and neuroblastoma cell lines, RAS/RAF/MEK/ERK MAP kinase antagonism is not the primary mechanism by which rigosertib exerts cytotoxic effects in this context. Interestingly, many kinase inhibitors, including the MET inhibitor tivanitinib, the PI3 kinase inhibitor buparlisib, and the SRC inhibitor KX2-361, also affect microtubule function (44-46). Rigosertib, then, may function as both a microtubule destabilizing agent and a RAS mimetic in some cellular contexts.

Inhibitors of microtubule polymerization, particularly the vinca alkaloids vincristine and vinorelbine, are commonly used in the treatment of pediatric RMS and NB. Vincristine in combination with other agents comprises the standard-of-care chemotherapeutic regimen for the upfront treatment of low- (47), intermediate- (48), and high-risk RMS (44). Vincristine is also one of the chemotherapeutics used in the induction of remission in patients newly-diagnosed with high-risk NB (49) and in the treatment of primary refractory NB (50). Vinorelbine is part of the maintenance chemotherapy regimens used in RMS treatment (51) and is combined with temsirolimus in the treatment of RMS patients in first relapse (52). The clinical use of the vinca alkaloids is complicated by several debilitating adverse effects including peripheral neuropathy (53). In addition, other chemotherapeutics that interact with tubulin, such as nab-paclitaxel (54) and eribulin (55), have promising preclinical activity in RMS models. Although no pediatric clinical trials of rigosertib have currently been conducted, the side effect profile of rigosertib in adult trials has been favorable compared to that of the vinca alkaloids. Peripheral neuropathy has not been noted as an adverse event associated with rigosertib treatment. In fact, the most commonly reported adverse events reported in trials of oral rigosertib were dysuria, hematuria, nausea, fatigue and diarrhea, all of which were reversible with discontinuation of the drug (8). Thus, rigosertib might represent a better-tolerated alternative to vinca alkaloids in the treatment of RMS and NB. The efficacy of rigosertib could be augmented by combination with

conventional chemotherapeutics or molecularly targeted agents, such as trametinib, which we investigated in this study.

In conclusion, rigosertib potently decreases viability of pediatric solid tumor cancer cells *in vitro* through its ability to interact with tubulin. Alternate methods of administration that might improve the intratumoral penetration of rigosertib and combining rigosertib with other agents such as trametinib merit further investigation.

Acknowledgements: The authors are grateful to D. Ritt, C. Thiele, B. Widemann, J. Glod, and P. Reddy for helpful discussions and review of the manuscript. This research was supported by the Intramural Research Program of the NIH: CJT is supported by the intramural research program of the National Center for Advancing Translational Sciences, DLS is supported by the intramural research program of the Eunice Kennedy Shriver National Institute of Child Health and Human Development and DKM, AEK, PAR, CMH, and MEY (ZIA BC 011805) are supported by the intramural research program of the National Cancer Institute. MEY is also supported by a YIA from the Alex's Lemonade Stand Foundation. This project has been funded in part with Federal funds from the National Cancer Institute, National Institutes of Health, under Contract No. 75N91019D00024. The content of this publication does not necessarily reflect the views or policies of the Department of Health and Human Services, nor does mention of trade names, commercial products, or organizations imply endorsement by the U.S. Government.

REFERENCES

1. Gumireddy K, Reddy MV, Cosenza SC, Boominathan R, Baker SJ, Papathi N*, et al.* ON01910, a non-ATP-competitive small molecule inhibitor of Plk1, is a potent anticancer agent. Cancer Cell **2005**;7(3):275-86 doi 10.1016/j.ccr.2005.02.009.
2. Athuluri-Divakar SK, Vasquez-Del Carpio R, Dutta K, Baker SJ, Cosenza SC, Basu I*, et al.* A Small Molecule RAS-Mimetic Disrupts RAS Association with Effector Proteins to Block Signaling. Cell **2016**;165(3):643-55 doi 10.1016/j.cell.2016.03.045.
3. Ritt DA, Abreu-Blanco MT, Bindu L, Durrant DE, Zhou M, Specht SI*, et al.* Inhibition of Ras/Raf/MEK/ERK Pathway Signaling by a Stress-Induced Phospho-Regulatory Circuit. Mol Cell **2016**;64(5):875-87 doi 10.1016/j.molcel.2016.10.029.
4. Baker SJ, Cosenza SC, Athuluri-Divakar S, Reddy MVR, Vasquez-Del Carpio R, Jain R*, et al.* A Contaminant Impurity, Not Rigosertib, Is a Tubulin Binding Agent. Mol Cell **2020**;79(1):180-90 e4 doi 10.1016/j.molcel.2020.05.024.
5. Jost M, Chen Y, Gilbert LA, Horlbeck MA, Krenning L, Menchon G*, et al.* Combined CRISPRi/a-Based Chemical Genetic Screens Reveal that Rigosertib Is a Microtubule-Destabilizing Agent. Mol Cell **2017**;68(1):210-23 e6 doi 10.1016/j.molcel.2017.09.012.
6. Jost M, Chen Y, Gilbert LA, Horlbeck MA, Krenning L, Menchon G*, et al.* Pharmaceutical-Grade Rigosertib Is a Microtubule-Destabilizing Agent. Mol Cell **2020**;79(1):191-8 e3 doi 10.1016/j.molcel.2020.06.008.
7. Baker SJ, Cosenza SC, Ramana Reddy MV, Premkumar Reddy E. Rigosertib ameliorates the effects of oncogenic KRAS signaling in a murine model of myeloproliferative neoplasia. Oncotarget **2019**;10(20):1932-42 doi 10.18632/oncotarget.26735.
8. Bowles DW, Diamond JR, Lam ET, Weekes CD, Astling DP, Anderson RT*, et al.* Phase I study of oral rigosertib (ON 01910.Na), a dual inhibitor of the PI3K and Plk1 pathways, in adult patients with advanced solid malignancies. Clin Cancer Res **2014**;20(6):1656-65 doi 10.1158/1078-0432.CCR-13-2506.
9. Jimeno A, Li J, Messersmith WA, Laheru D, Rudek MA, Maniar M*, et al.* Phase I study of ON 01910.Na, a novel modulator of the Polo-like kinase 1 pathway, in adult patients with solid tumors. J Clin Oncol **2008**;26(34):5504-10 doi 10.1200/JCO.2008.17.9788.
10. Ma WW, Messersmith WA, Dy GK, Weekes CD, Whitworth A, Ren C*, et al.* Phase I study of Rigosertib, an inhibitor of the phosphatidylinositol 3-kinase and Polo-like kinase 1 pathways, combined with gemcitabine in patients with solid tumors and pancreatic cancer. Clin Cancer Res **2012**;18(7):2048-55 doi 10.1158/1078-0432.CCR-11-2813.
11. Garcia-Manero G, Fenaux P, Al-Kali A, Baer MR, Sekeres MA, Roboz GJ*, et al.* Rigosertib versus best supportive care for patients with high-risk myelodysplastic syndromes after failure of hypomethylating drugs (ONTIME): a randomised, controlled, phase 3 trial. Lancet Oncol **2016**;17(4):496-508 doi 10.1016/S1470-2045(16)00009-7.
12. Komrokji RS, Raza A, Lancet JE, Ren C, Taft D, Maniar M*, et al.* Phase I clinical trial of oral rigosertib in patients with myelodysplastic syndromes. Br J Haematol **2013**;162(4):517-24 doi 10.1111/bjh.12436.
13. Silverman LR, Greenberg P, Raza A, Olnes MJ, Holland JF, Reddy P*, et al.* Clinical activity and safety of the dual pathway inhibitor rigosertib for higher risk myelodysplastic syndromes following DNA methyltransferase inhibitor therapy. Hematol Oncol **2015**;33(2):57-66 doi 10.1002/hon.2137.
14. O'Neil BH, Scott AJ, Ma WW, Cohen SJ, Leichman L, Aisner DL*, et al.* A phase II/III randomized study to compare the efficacy and safety of rigosertib plus gemcitabine

versus gemcitabine alone in patients with previously untreated metastatic pancreatic cancer. Ann Oncol **2015**;26(9):1923-9 doi 10.1093/annonc/mdv264.
15. Shern JF, Chen L, Chmielecki J, Wei JS, Patidar R, Rosenberg M*, et al.* Comprehensive genomic analysis of rhabdomyosarcoma reveals a landscape of alterations affecting a common genetic axis in fusion-positive and fusion-negative tumors. Cancer Discov **2014**;4(2):216-31 doi 10.1158/2159-8290.CD-13-0639.
16. Brohl AS, Kahen E, Yoder SJ, Teer JK, Reed DR. The genomic landscape of malignant peripheral nerve sheath tumors: diverse drivers of Ras pathway activation. Sci Rep **2017**;7(1):14992 doi 10.1038/s41598-017-15183-1.
17. Eleveld TF, Schild L, Koster J, Zwijnenburg DA, Alles LK, Ebus ME*, et al.* RAS-MAPK Pathway-Driven Tumor Progression Is Associated with Loss of CIC and Other Genomic Aberrations in Neuroblastoma. Cancer Res **2018**;78(21):6297-307 doi 10.1158/0008-5472.CAN-18-1045.
18. Huang SC, Alaggio R, Sung YS, Chen CL, Zhang L, Kao YC*, et al.* Frequent HRAS Mutations in Malignant Ectomesenchymoma: Overlapping Genetic Abnormalities With Embryonal Rhabdomyosarcoma. Am J Surg Pathol **2016**;40(7):876-85 doi 10.1097/PAS.0000000000000612.
19. Irving J, Matheson E, Minto L, Blair H, Case M, Halsey C*, et al.* Ras pathway mutations are prevalent in relapsed childhood acute lymphoblastic leukemia and confer sensitivity to MEK inhibition. Blood **2014**;124(23):3420-30 doi 10.1182/blood-2014-04-531871.
20. Hettmer S, Wagers AJ. Muscling in: Uncovering the origins of rhabdomyosarcoma. Nat Med **2010**;16(2):171-3 doi 10.1038/nm0210-171.
21. Tsubota S, Kadomatsu K. Origin and mechanism of neuroblastoma. Oncoscience **2017**;4(7-8):70-2 doi 10.18632/oncoscience.360.
22. Dyrager C, Mollers LN, Kjall LK, Alao JP, Diner P, Wallner FK*, et al.* Design, synthesis, and biological evaluation of chromone-based p38 MAP kinase inhibitors. J Med Chem **2011**;54(20):7427-31 doi 10.1021/jm200818j.
23. McLoughlin EC, O'Boyle NM. Colchicine-Binding Site Inhibitors from Chemistry to Clinic: A Review. Pharmaceuticals (Basel) **2020**;13(1) doi 10.3390/ph13010008.
24. Shevchenko A, Tomas H, Havlis J, Olsen JV, Mann M. In-gel digestion for mass spectrometric characterization of proteins and proteomes. Nat Protoc **2006**;1(6):2856-60 doi 10.1038/nprot.2006.468.
25. Foucquier J, Guedj M. Analysis of drug combinations: current methodological landscape. Pharmacol Res Perspect **2015**;3(3):e00149 doi 10.1002/prp2.149.
26. Khanna C, Prehn J, Yeung C, Caylor J, Tsokos M, Helman L. An orthotopic model of murine osteosarcoma with clonally related variants differing in pulmonary metastatic potential. Clinical & experimental metastasis **2000**;18(3):261-71.
27. Sinha S, Field JJ, Miller JH. Use of substitute Nonidet P-40 nonionic detergents in intracellular tubulin polymerization assays for screening of microtubule targeting agents. Biochem Cell Biol **2017**;95(3):379-84 doi 10.1139/bcb-2016-0141.
28. Lin GL, Wilson KM, Ceribelli M, Stanton BZ, Woo PJ, Kreimer S*, et al.* Therapeutic strategies for diffuse midline glioma from high-throughput combination drug screening. Sci Transl Med **2019**;11(519) doi 10.1126/scitranslmed.aaw0064.
29. Yohe ME, Gryder BE, Shern JF, Song YK, Chou HC, Sindiri S*, et al.* MEK inhibition induces MYOG and remodels super-enhancers in RAS-driven rhabdomyosarcoma. Sci Transl Med **2018**;10(448) doi 10.1126/scitranslmed.aan4470.
30. Vaseva AV, Yohe ME. Targeting RAS in pediatric cancer: is it becoming a reality? Curr Opin Pediatr **2020**;32(1):48-56 doi 10.1097/MOP.0000000000000856.
31. Drosten M, Dhawahir A, Sum EY, Urosevic J, Lechuga CG, Esteban LM*, et al.* Genetic analysis of Ras signalling pathways in cell proliferation, migration and survival. EMBO J **2010**;29(6):1091-104 doi 10.1038/emboj.2010.7.

32. Urasaki Y, Fiscus RR, Le TT. Detection of the Cell Cycle-Regulated Negative Feedback Phosphorylation of Mitogen-Activated Protein Kinases in Breast Carcinoma using Nanofluidic Proteomics. Sci Rep **2018**;8(1):9991 doi 10.1038/s41598-018-28335-8.
33. Chapman CM, Sun X, Roschewski M, Aue G, Farooqui M, Stennett L*, et al.* ON 01910.Na is selectively cytotoxic for chronic lymphocytic leukemia cells through a dual mechanism of action involving PI3K/AKT inhibition and induction of oxidative stress. Clin Cancer Res **2012**;18(7):1979-91 doi 10.1158/1078-0432.CCR-11-2113.
34. Loor G, Kondapalli J, Schriewer JM, Chandel NS, Vanden Hoek TL, Schumacker PT. Menadione triggers cell death through ROS-dependent mechanisms involving PARP activation without requiring apoptosis. Free Radic Biol Med **2010**;49(12):1925-36 doi 10.1016/j.freeradbiomed.2010.09.021.
35. Kumar S, Jiang MS, Adams JL, Lee JC. Pyridinylimidazole compound SB 203580 inhibits the activity but not the activation of p38 mitogen-activated protein kinase. Biochem Biophys Res Commun **1999**;263(3):825-31 doi 10.1006/bbrc.1999.1454.
36. Frantz B, Klatt T, Pang M, Parsons J, Rolando A, Williams H*, et al.* The activation state of p38 mitogen-activated protein kinase determines the efficiency of ATP competition for pyridinylimidazole inhibitor binding. Biochemistry **1998**;37(39):13846-53 doi 10.1021/bi980832y.
37. Cocker HA, Hobbs SM, Tiffin N, Pritchard-Jones K, Pinkerton CR, Kelland LR. High levels of the MDM2 oncogene in paediatric rhabdomyosarcoma cell lines may confer multidrug resistance. Br J Cancer **2001**;85(11):1746-52 doi 10.1054/bjoc.2001.2145.
38. Patterson JC, Joughin BA, van de Kooij B, Lim DC, Lauffenburger DA, Yaffe MB. ROS and Oxidative Stress Are Elevated in Mitosis during Asynchronous Cell Cycle Progression and Are Exacerbated by Mitotic Arrest. Cell Syst **2019**;8(2):163-7 e2 doi 10.1016/j.cels.2019.01.005.
39. Powers SK, Ji LL, Kavazis AN, Jackson MJ. Reactive oxygen species: impact on skeletal muscle. Compr Physiol **2011**;1(2):941-69 doi 10.1002/cphy.c100054.
40. Chen X, Stewart E, Shelat AA, Qu C, Bahrami A, Hatley M*, et al.* Targeting oxidative stress in embryonal rhabdomyosarcoma. Cancer Cell **2013**;24(6):710-24 doi 10.1016/j.ccr.2013.11.002.
41. Hedrick E, Crose L, Linardic CM, Safe S. Histone Deacetylase Inhibitors Inhibit Rhabdomyosarcoma by Reactive Oxygen Species-Dependent Targeting of Specificity Protein Transcription Factors. Mol Cancer Ther **2015**;14(9):2143-53 doi 10.1158/1535-7163.MCT-15-0148.
42. Kefaloyianni E, Gaitanaki C, Beis I. ERK1/2 and p38-MAPK signalling pathways, through MSK1, are involved in NF-kappaB transactivation during oxidative stress in skeletal myoblasts. Cell Signal **2006**;18(12):2238-51 doi 10.1016/j.cellsig.2006.05.004.
43. Hart LS, Rader J, Raman P, Batra V, Russell MR, Tsang M*, et al.* Preclinical Therapeutic Synergy of MEK1/2 and CDK4/6 Inhibition in Neuroblastoma. Clin Cancer Res **2017**;23(7):1785-96 doi 10.1158/1078-0432.CCR-16-1131.
44. Arndt CA, Stoner JA, Hawkins DS, Rodeberg DA, Hayes-Jordan AA, Paidas CN*, et al.* Vincristine, actinomycin, and cyclophosphamide compared with vincristine, actinomycin, and cyclophosphamide alternating with vincristine, topotecan, and cyclophosphamide for intermediate-risk rhabdomyosarcoma: children's oncology group study D9803. J Clin Oncol **2009**;27(31):5182-8 doi 10.1200/JCO.2009.22.3768.
45. Smolinski MP, Bu Y, Clements J, Gelman IH, Hegab T, Cutler DL*, et al.* Discovery of Novel Dual Mechanism of Action Src Signaling and Tubulin Polymerization Inhibitors (KX2-391 and KX2-361). J Med Chem **2018**;61(11):4704-19 doi 10.1021/acs.jmedchem.8b00164.
46. Tanabe K. Microtubule Depolymerization by Kinase Inhibitors: Unexpected Findings of Dual Inhibitors. Int J Mol Sci **2017**;18(12) doi 10.3390/ijms18122508.

47. Walterhouse DO, Pappo AS, Meza JL, Breneman JC, Hayes-Jordan AA, Parham DM*, et al.* Shorter-duration therapy using vincristine, dactinomycin, and lower-dose cyclophosphamide with or without radiotherapy for patients with newly diagnosed low-risk rhabdomyosarcoma: a report from the Soft Tissue Sarcoma Committee of the Children's Oncology Group. J Clin Oncol **2014**;32(31):3547-52 doi 10.1200/JCO.2014.55.6787.
48. Hawkins DS, Chi YY, Anderson JR, Tian J, Arndt CAS, Bomgaars L*, et al.* Addition of Vincristine and Irinotecan to Vincristine, Dactinomycin, and Cyclophosphamide Does Not Improve Outcome for Intermediate-Risk Rhabdomyosarcoma: A Report From the Children's Oncology Group. J Clin Oncol **2018**;36(27):2770-7 doi 10.1200/JCO.2018.77.9694.
49. Kushner BH, Kramer K, LaQuaglia MP, Modak S, Yataghene K, Cheung NK. Reduction from seven to five cycles of intensive induction chemotherapy in children with high-risk neuroblastoma. J Clin Oncol **2004**;22(24):4888-92 doi 10.1200/JCO.2004.02.101.
50. Kushner BH, Kramer K, Modak S, Yataghene K, Cheung NK. High-dose cyclophosphamide-irinotecan-vincristine for primary refractory neuroblastoma. Eur J Cancer **2011**;47(1):84-9 doi 10.1016/j.ejca.2010.09.014.
51. Bisogno G, De Salvo GL, Bergeron C, Gallego Melcon S, Merks JH, Kelsey A*, et al.* Vinorelbine and continuous low-dose cyclophosphamide as maintenance chemotherapy in patients with high-risk rhabdomyosarcoma (RMS 2005): a multicentre, open-label, randomised, phase 3 trial. Lancet Oncol **2019**;20(11):1566-75 doi 10.1016/S1470-2045(19)30617-5.
52. Mascarenhas L, Chi YY, Hingorani P, Anderson JR, Lyden ER, Rodeberg DA*, et al.* Randomized Phase II Trial of Bevacizumab or Temsirolimus in Combination With Chemotherapy for First Relapse Rhabdomyosarcoma: A Report From the Children's Oncology Group. J Clin Oncol **2019**;37(31):2866-74 doi 10.1200/JCO.19.00576.
53. Mora E, Smith EM, Donohoe C, Hertz DL. Vincristine-induced peripheral neuropathy in pediatric cancer patients. Am J Cancer Res **2016**;6(11):2416-30.
54. Zhang L, Marrano P, Kumar S, Leadley M, Elias E, Thorner P*, et al.* Nab-paclitaxel is an active drug in preclinical model of pediatric solid tumors. Clin Cancer Res **2013**;19(21):5972-83 doi 10.1158/1078-0432.CCR-13-1485.
55. Kolb EA, Gorlick R, Reynolds CP, Kang MH, Carol H, Lock R*, et al.* Initial testing (stage 1) of eribulin, a novel tubulin binding agent, by the pediatric preclinical testing program. Pediatr Blood Cancer **2013**;60(8):1325-32 doi 10.1002/pbc.24517.

FIGURE LEGENDS

Figure 1: Rigosertib decreases cell viability in rhabdomyosarcoma and neuroblastoma cell lines. **(A)** Efficacy of rigosertib was determined in rhabdomyosarcoma cell lines using percent confluence 72 hours after treatment with rigosertib as a marker of viability. Percent confluence was determined by live cell imaging (Incucyte ZOOM). Points represent the mean and error bars show the standard error of the mean of triplicate measurements. Curves in red are cell lines with mutant NRAS (RD) or HRAS (SMS-CTR, BIRCH). Curves in blue are cell lines expressing wild-type RAS isoforms (RH4, RH30, RMS-YM). **(B)** Efficacy of rigosertib was determined in neuroblastoma cell lines using percent confluence 96 hours after treatment with rigosertib as a marker of viability. Curves in red are cell lines expressing mutant NRAS (SKNAS) or KRAS (NBEB). Curves in blue are cell lines expressing wild-type RAS isoforms (SHEP, IMR5). **(C)** Efficacy of rigosertib was determined in a panel of isogeneic RAS-dependent MEFs. In this experiment, percent confluence 72 hours after treatment with rigosertib was used as a marker of viability. **(D)** Quantification of 14-day clonogenic assays for RD, SMS-CTR, SKNAS, CHP212, and RH30 growth in the presence of rigosertib. * denotes $p < 0.05$, ** denotes $p < 0.001$ as determined by Student's t-test. **(E)** Relative potency of rigosertib (top) and the MEK inhibitor trametinib (bottom) as represented by the z-score of the area under the dose-response curve (AUC) in a panel of cell lines screened as part of a collaboration between NCI and NCATS for RAS wild-type and RAS-mutant cells. P-values determined by Mann-Whitney test.

Figure 2: Rigosertib induces apoptosis and G2/M-phase arrest in RAS-mutant rhabdomyosarcoma and neuroblastoma cell lines. **(A)** Caspase 3/7 activity, determined by Caspase-Glo, 18 hours after rigosertib treatment of the indicated rhabdomyosarcoma (RD or SMS-CTR) cell lines. * denotes $p < 0.01$, ** denotes $p < 0.001$ for comparison with DMSO, as determined by 2-way ANOVA with Tukey's multiple comparison test. **(B)** RD or SMS-CTR cells were treated with DMSO or 2 μM rigosertib for 48 hours, after which cells were stained with Annexin/Sytox green and analyzed by flow cytometry. Percent apoptotic cells were defined as cells that were annexin positive and Sytox positive or negative. * denotes $p < 0.001$ and ** denotes $p < 0.0001$ as determined by 2-way ANOVA with Sidak's multiple comparison test. **(C)** Treatment with 2 μM rigosertib for 24 hours induces G2/M arrest in rhabdomyosarcoma (top) or neuroblastoma (bottom) cells as determined by DNA content analysis. **(D)** Treatment with 2 μM rigosertib for 24 hours induces mitotic arrest in rhabdomyosarcoma (RD and SMS-CTR, top) or

neuroblastoma (SKNAS and NBEB, bottom) cells as determined by phosphorylated histone H3 immunoblot. **(E)** Treatment with 250 nM rigosertib for 24 hours induces mitotic arrest in RD (top) and SKNAS (bottom) cells as determined by phosphorylated histone H3 immunofluorescence. Representative images are shown. Quantification of 7 independent fields shown at right. * denotes $p < 0.05$, ** denotes $p < 0.001$ as determined by 2-way ANOVA with Sidak's multiple comparison test.

Figure 3: Rigosertib treatment does not inhibit RAS/MAPK or PI3K/AKT signaling in rhabdomyosarcoma cell lines. **(A)** RD (left) or SMS-CTR (right) rhabdomyosarcoma cells were serum starved in 2% HS and treated with DMSO or 2 μM rigosertib for 24 hours prior to stimulation with either vehicle or 20 ng/mL IGF1 for 30 minutes. Treated cells were harvested and the resulting cell lysates were blotted for phosphorylated ERK1/2, total ERK 1/2, pS473 AKT and total AKT. **(B)** Immunoblot analysis of total and phosphorylated forms of MEK1 and ERK1/2 from RD cells treated with either 1 μM rigosertib, 100 nM trametinib (MEK inhibitor) or the combination of 1 μM rigosertib and 100 nM trametinib for 6 hours. Kinases responsible for phosphorylation of each residue studied are indicated by italics. Activating phosphorylation events are highlighted in bold. **(C)** SKNAS cells were serum starved in 0.5% FBS and treated with DMSO or 2 μM rigosertib for 24 hours prior to stimulation with either vehicle or 20 ng/mL IGF1 for 5 minutes. Treated cells were harvested and the resulting cell lysates were blotted for phosphorylated ERK1/2, total ERK 1/2, pS473 AKT and total AKT. **(D)** Immunoblot analysis of total and phosphorylated forms of MEK1 and ERK1/2 from SKNAS cells treated with either 1 μM rigosertib, 100 nM trametinib or the combination of 1 μM rigosertib and 100 nM trametinib for 6 hours. **(E)** Matrix plot (8x11) for the combination of trametinib (0-1000 nM) and rigosertib (0-10 μM) in both viability (top, percent confluence) and Δ Bliss (bottom) format in RD cells. **(F)** Cell confluence as a function of time for RD cells treated with vehicle, 30 nM trametinib, 1 μM rigosertib, or the combination.

Figure 4: The cell cycle block induced by rigosertib treatment in RMS cells promotes generation of reactive oxygen species and activation of the stress MAP kinase cascades in rhabdomyosarcoma cells. **(A)** Immunoblot analysis of phosphorylated p38 (p-p38), phosphorylated MKK4, and cleaved PARP of RD (left) or SMS-CTR (right) cells treated with 2 μM rigosertib with or without the 10 mM N-acetylcysteine (NAC) for 18 hours. **(B)** Immunoblot analysis of p-p38, p-MAPKAPK2 (a p38 substrate), total MAPKAPK2, and cleaved PARP of RD (left) or SMS-CTR (right) cells treated with 2 μM rigosertib with or without co-treatment with 20

μM SB-203580 (a p38 inhibitor) for 18 hours. **(C)** NAC co-treatment does not prevent rigosertib-induced G2/M arrest in RD (top) or SMS-CTR (bottom) as determined by DNA content analysis after 24 hours of treatment. **(D)** SB-203580 co-treatment does not prevent rigosertib-induced G2/M arrest in RD (top) or SMS-CTR (bottom) as determined by DNA content analysis after 24 hours of treatment. **(E)** NAC co-treatment does not prevent rigosertib-induced caspase 3/7 activity in RD (left) or SMS-CTR (right) as determined by Caspase-glo after 18 hours of treatment. * denotes $p < 0.05$, ns denotes not significant, as determined by 2-way ANOVA with Tukey's correction for multiple comparisons. **(F)** SB-203580 co-treatment does not prevent rigosertib-induced caspase 3/7 activity in RD (left) or SMS-CTR (right) as determined by Caspase-glo after 18 hours of treatment. ns denotes not significant as determined by 2-way ANOVA with Tukey's correction for multiple comparisons.

Figure 5: Rigosertib interacts with tubulin in RMS cells, which destabilizes microtubules and induces mitotic spindle defects. **(A)** Treatment of RD or SKNAS with 2 μM rigosertib for 24 hours decreases acetylation of α-tubulin as determined by quantitative capillary immunoassay. **(B)** RD (top) or SKNAS (bottom) were treated with increasing concentrations of rigosertib for 4 hours prior to lysis and separation of polymerized (P) and soluble (S) tubulin by centrifugation. The pellets were resuspended in a volume equal to that of the soluble fraction. Equal volumes of P and S for each condition were subjected to SDS-PAGE and immunoblot for α-tubulin. **(C)** Treatment of RD (top) or SKNAS (bottom) with 250 nM rigosertib for 24 hours induces mitotic spindle defects in unsynchronized cells, as determined by immunofluorescence staining of α-tubulin (mitotic spindles) and pericentrin (centrosomes). Representative images are shown. Boxed insets are shown as zoomed images at right and display multipolar mitotic spindles and other spindle defects.

Figure 6: Rigosertib delays time to tumor progression in an RD xenograft model. **(A)** Tumor volume on day 19 after initiation of vehicle or rigosertib (150 mg/kg IP twice daily) treatment of severe combined immunodeficient (SCID) beige mice bearing orthotopic RD xenografts. Tumors are significantly smaller in the rigosertib treated group compared to the vehicle group ($p = 0.0397$, Student's t-test). **(B)** Rigosertib treatment significantly prolongs survival, denoted as time to develop a tumor of greater than 2 cm^3 ($p = 0.0111$, Mantel-Cox test). **(C)** Rigosertib treatment did not decrease mouse body weight by more than 20% in RD xenograft models (dashed line). **(D)** Rigosertib treatment did not decrease α-tubulin acetylation

in RD xenografts, a pharmacodynamic indicator of response to the drug, indicating poor tumor penetration of the drug.

Figure 1

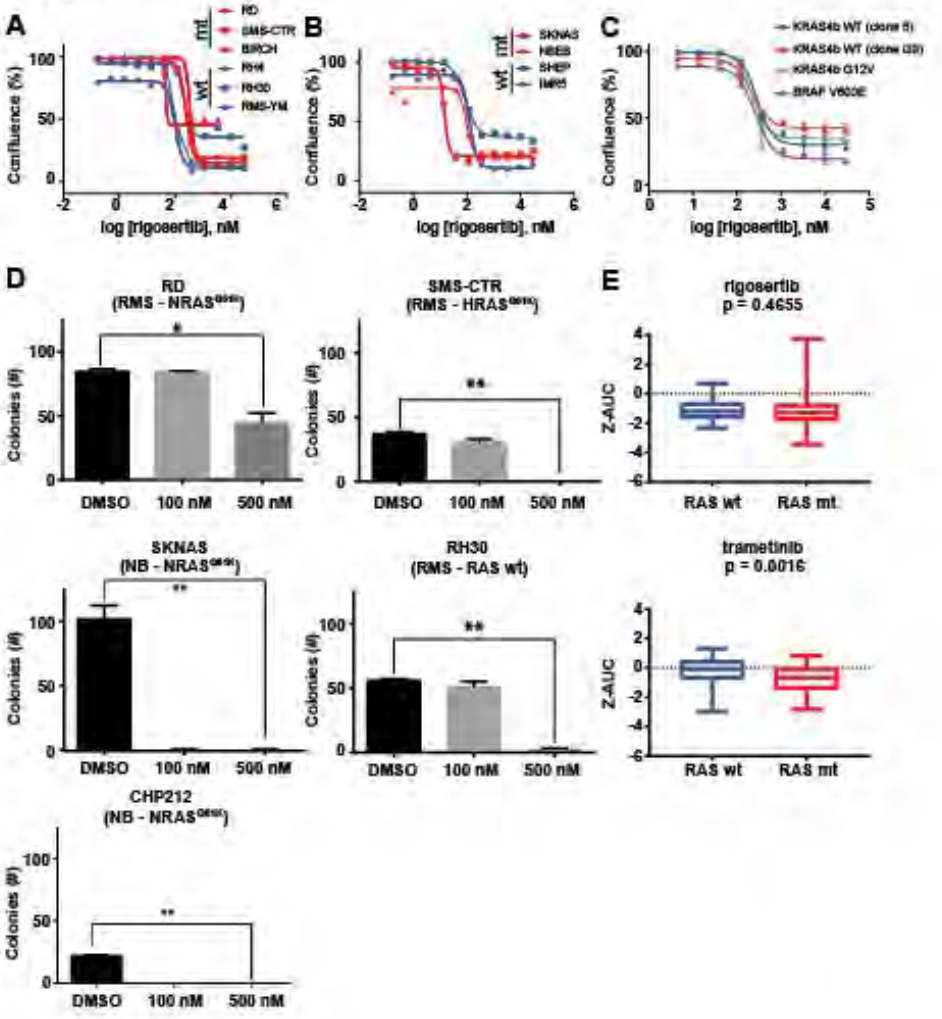

Figure 2

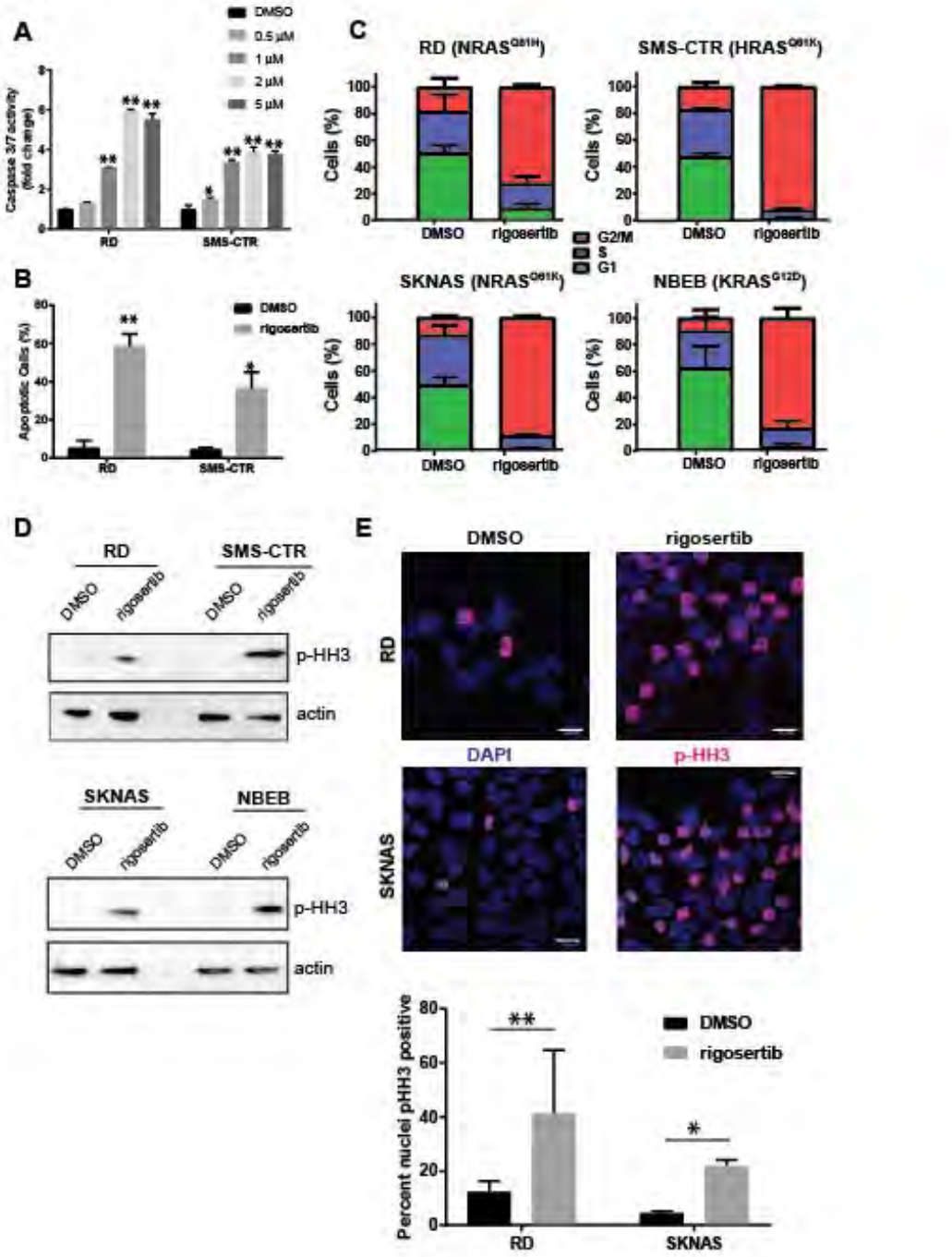

Figure 3

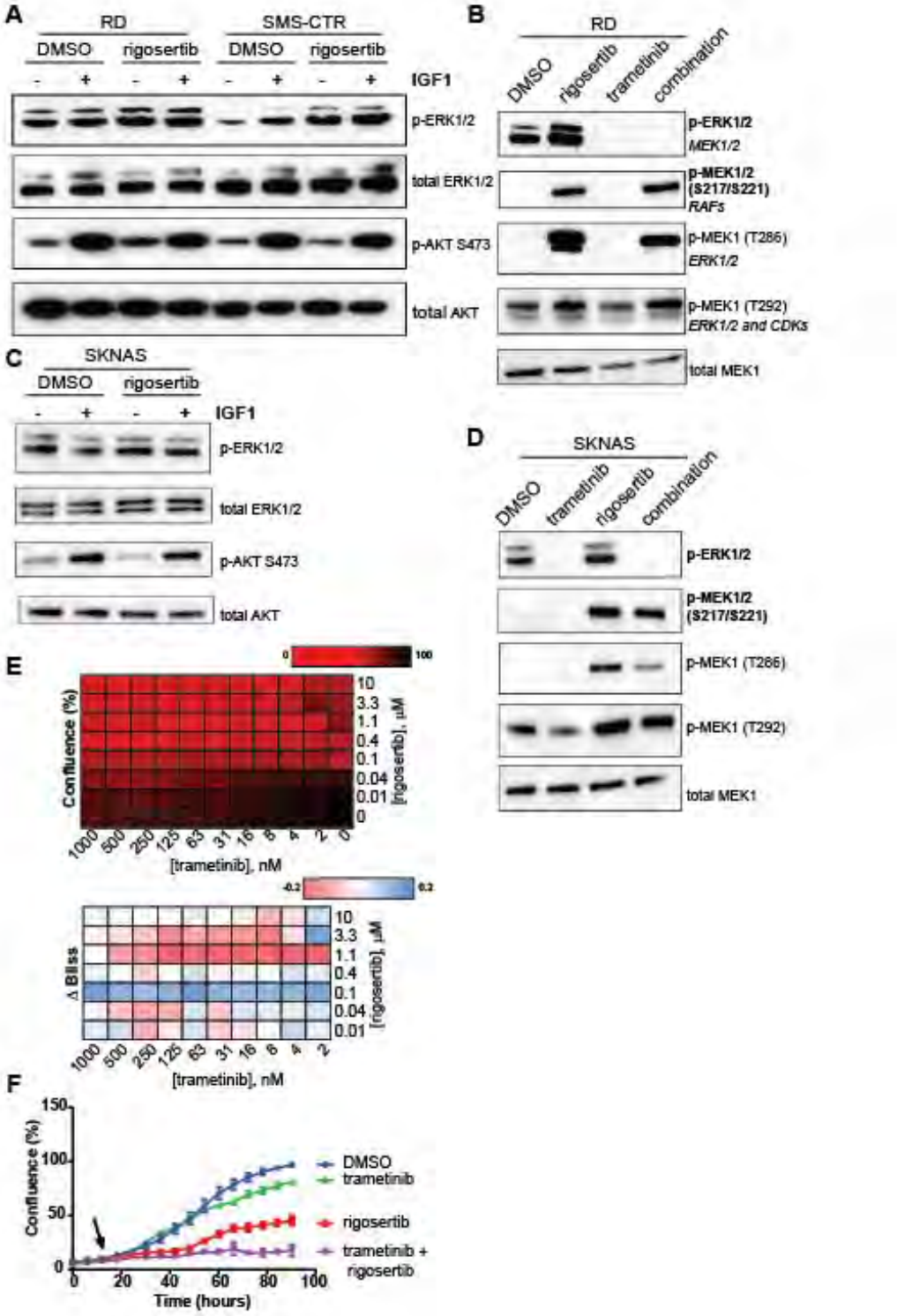

Figure 4

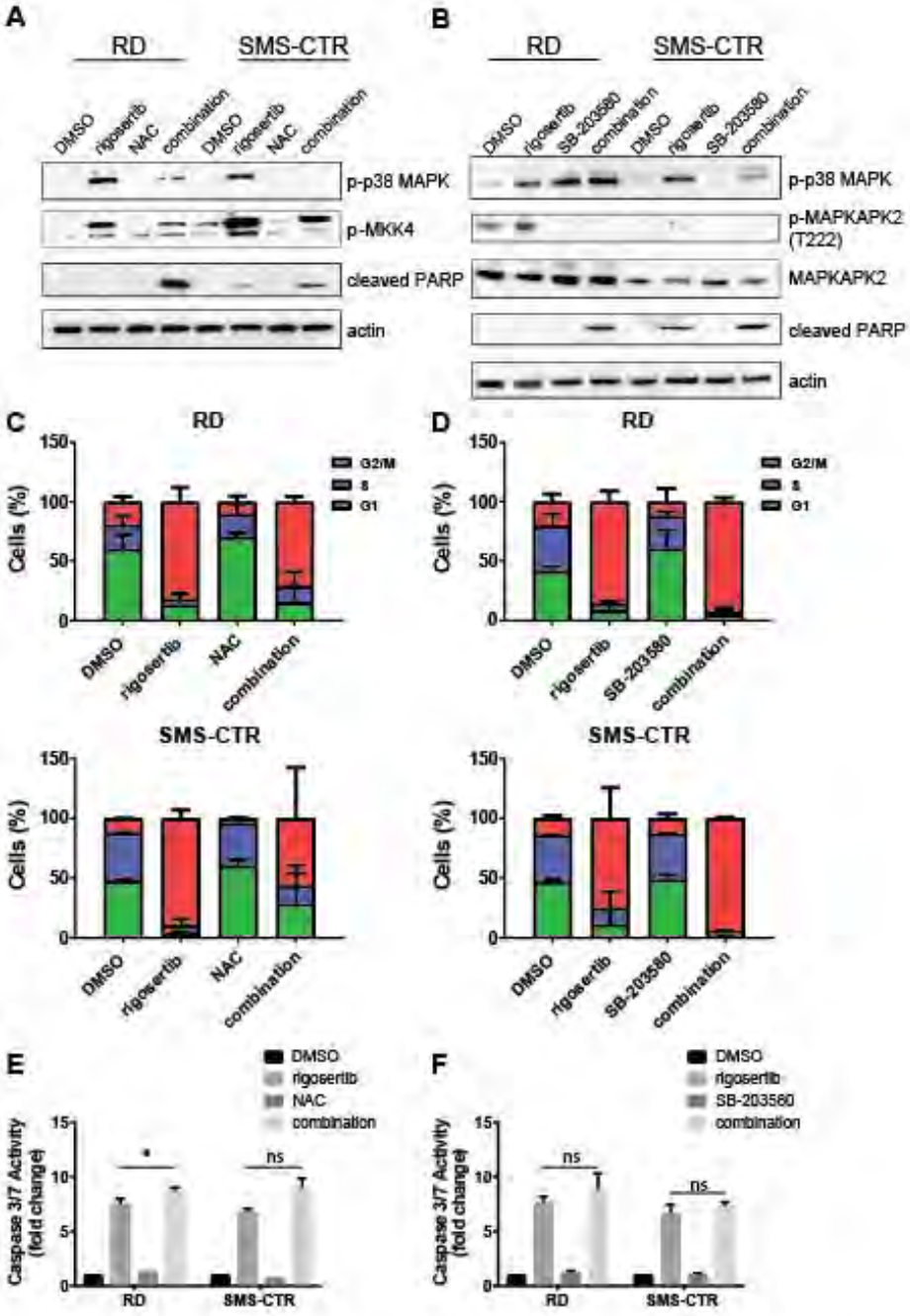

Figure 5

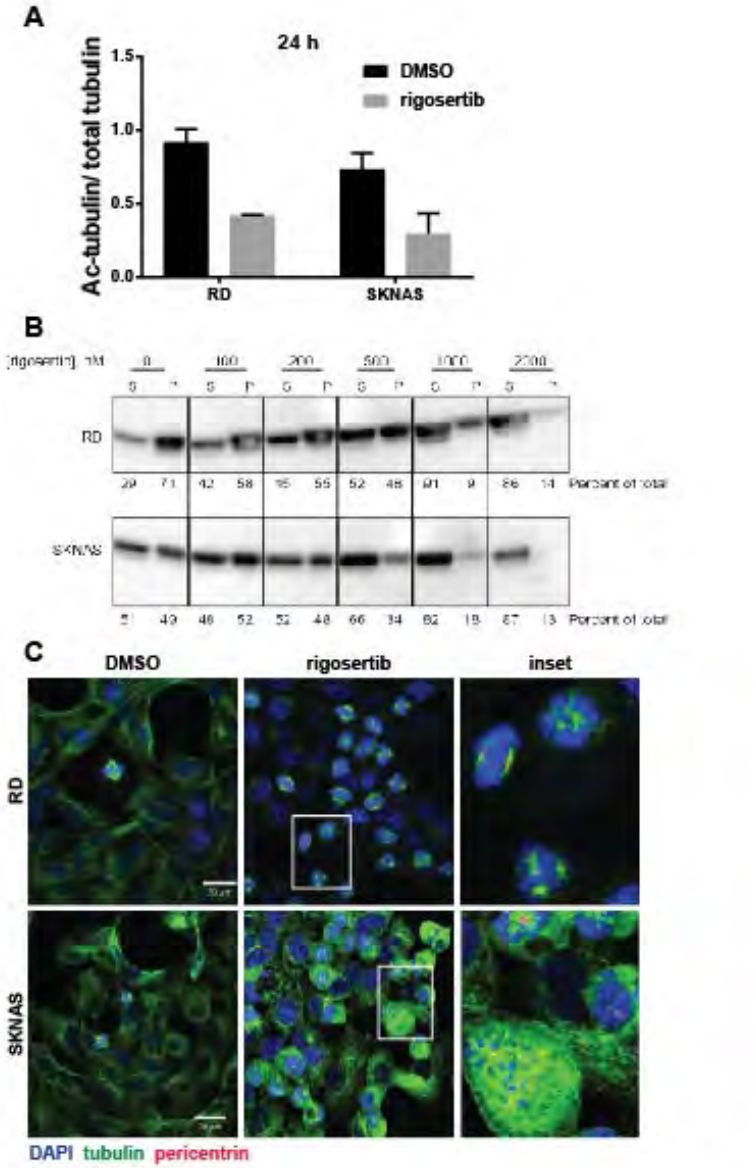

Figure 6

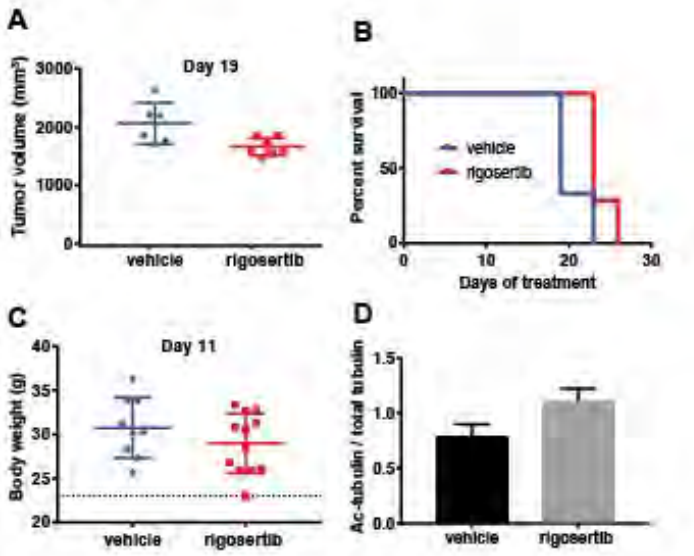

AACR American Association for Cancer Research

Molecular Cancer Therapeutics

Rigosertib induces mitotic arrest and apoptosis in RAS-driven rhabdomyosarcoma and neuroblastoma

Joshua T. Kowalczyk, Xiaolin Wan, Edjay R. Hernandez, et al.

Mol Cancer Ther Published OnlineFirst November 6, 2020.